Arabian Journal for Science and Engineering (2024) 49:11523–11540
https://doi.org/10.1007/s13369-023-08658-z

RESEARCH ARTICLE-MECHANICAL ENGINEERING

Optimization for Bending Collapse of Thin-Walled Twelve Right-Angle Section Tubes with Variable Thickness

Xi Liu[1] · Rui Liang[2] · Yuanzhi Hu[1]

Received: 25 September 2023 / Accepted: 18 December 2023 / Published online: 7 February 2024

Abstract
This study aimed to investigate the influence of variable thickness on the mechanical properties of thin-walled twelve right-angle section tubes (TTRSTs) through numerical characterization. This paper introduced the TTRSTs with different thicknesses for sides and webs. The three-point bending finite element model correlated with the physical test was built up and modified to find the lowest initial peak force (IPF), maximum specific energy absorption (SEA), and highest mean crushing force (MCF). Effects of variable thickness as well as impact location on the energy absorption performance of TTRSTs were investigated, suggesting that the energy absorption performance was more sensitive to side plate thickness changes than web plate thickness changes in web plate impacts. In addition, the TTRSTs with about 2.5 mm thickness demonstrated the highest SEA. Optimal Latin hypercube design (Opt LHD), response surface method (RSM), and NSGA-II were employed to optimize the TTRST multiobjectively under different impact loadings. The optimized results highlight that the TTRSTs can reach a 46.92% lower initial peak force or 2.61% higher MCF with minor SEA by selecting the appropriate thickness for impacts at different locations.

Keywords Bending collapse · Twelve right-angle section tubes · Energy absorption · Variable thickness · Multi-objective optimize

1 Introduction

Thin-walled structures (TWSs) that present excellent potential for balance between the energy absorption characteristic and lightweight are widely applied as energy absorption structures in various engineering fields, including automobiles, aircraft, and ships [1, 2]. Therefore, their energy characteristic under impact interests researchers for occupant safety considerations. The energy absorption performance of those metallic tubes under various load conditions has received extensive investigations [3], such as transverse bending [1, 4–7], axial impact [8–11], and lateral impact [12–15].

Among them, the bending impact of TWSs is one of the most common scenarios, making them a critical deformation mechanism to dissipate kinetic energy and protect passengers' safety under impact [16]. Under bend loading, the energy is mainly dissipated by static hinge lines, similar to the collapse mechanisms of TWSs subject to axial impact [17, 18]. Over the years, experimental [19–22], theoretical [23–27], and numerical [28–30] studies have been erected to gain a better understanding of TWS energy absorption performance. The hybrid artificial hummingbird-simulated annealing algorithm[31], slime mold algorithm and kriging surrogate model-based approach[32], multi-surrogate-assisted metaheuristics [33], and Non-Donminated Sorting Genetic Algorithm-II method (NSGA-II) [34] have been utilized by researchers in improving the crashworthiness of thin-walled structures. In addition, a range of TWSs with more desirable collapse modes has become increasingly prevalent in research [35]. For instance, Fu and Zhang [36] introduced and investigated a three-point bending of thin-walled arched beams with square sections. Wu et al. [37] investigated the circular multi-cell tubes subjected to

✉ Rui Liang
ruiliang@guat.edu.cn

1 Key Laboratory of Advanced Manufacture Technology for Automobile Parts, Ministry of Education, Chongqing University of Technology, Chongqing 400054, China

2 School of Automobile Engineering, Guilin University of Aerospace Technology, Guilin 541004, China

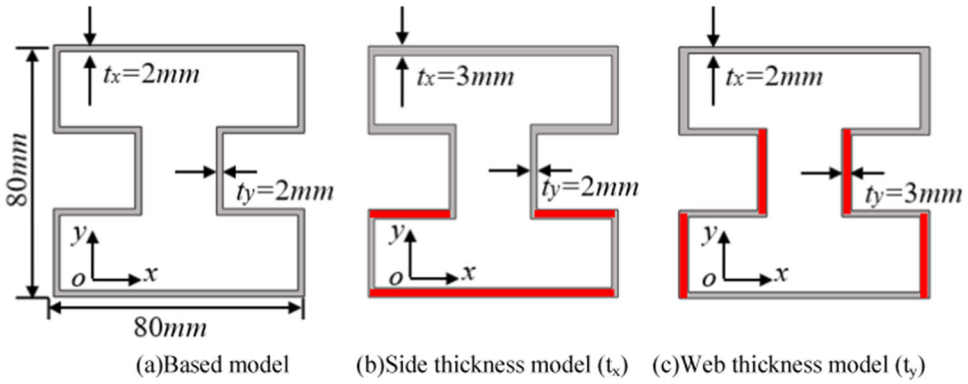

Fig. 1 Force versus displacement of the AA 6060 T4 TTRST tubes

bend loading. Researchers have introduced and used different cross section tubes as energy absorbers in vehicles to improve the energy absorption efficiency of square tubes subject to transverse bending [38].

Another current issue has concentrated on various section forms for their use as impact energy absorbers, a distinctive characteristic of square and circular cross sections mentioned above. For instance, Sun et al. [39, 40] conducted a parametric study to investigate the energy performance of the top-hat TWSs subjected to bending impact. Zhang et al. [41, 42] proposed to study the energy characteristic of the thin-walled twelve right-angle section tube (TTRST) subjected to bending impact. Their results reveal that the number of corners in a TWS cross section influences the energy absorption characteristic. Further, the TTRSTs have consequently been deemed preferable to the square cross section tube mentioned above since they can provide the required number of corners and better endure bending impact, directly improving crashworthiness.

All the aforementioned thin-walled structures, used extensively as energy absorbers, were built with the same thickness in the tubular radial direction. However, the shape cannot be consistently reinforced entirely [24]. As a result, those constructions with the same thickness around the shape might not use their materials and energy absorption to their full potential [43]. Besides, related research has shown that the thickness has a decisive influence on the crashworthiness performance of TWSs, and a structure with variable thickness has a good potential for showing a better energy absorption performance than that of the tubes with the same thickness [17]. Therefore, the walled thickness can be redesigned for thin-walled tubes that do not exhibit the optimal thickness distribution to improve the material utilization for achieving lightweight vehicular requirements. However, further studies on TTRSTs with variable thickness configurations have been lacking. It remains under-studied whether such TTRST with various thickness distributions could be further optimized for better material utilization and lightweight.

This paper proposed to provide new TTRSTs with variable thickness distribution to investigate their energy absorption characteristics. The initial peak force (IPF), specific energy absorption (SEA), and mean crushing force (MCF) were conducted as energy absorption indicators. The effect of the side plate and web plate thickness on TTRST's deformation modes and energy absorption characteristics were analyzed. Besides, the deformation modes and energy absorption of the TTRSTs with various thicknesses under side and web plate impact were performed, respectively. Further, the optimal design of the TTRSTs is obtained through multiobjective optimization. This paper is the first study investigating the dynamic response and multiobjective optimization of TTRSS with variable thickness distribution that could provide some valuable information for the effective design of TTRSTs with different geometrical parameters.

2 Energy Absorption Indicators

Structural energy absorption indicators should be defined to evaluate the energy absorption characteristic of TTRSS with variable thickness distribution subjected to bending impact. Initial peak force (IPF), specific energy absorption (SEA), and mean crushing force (MCF) are the most typical indicators used to evaluate crashworthiness [44–46]. It is anticipated that the IPF will be low while the SEA and MCF will be high, resulting in an excellent energy absorption performance. The IPF, SEA, and MCF can be denoted as follows [47]:

The energy absorbed (EA) can be expressed as:

$$\mathrm{EA} = \int_0^{\mathrm{d}} F(\mathrm{x})\mathrm{dx} \tag{1}$$

where d is the crushing distance, and $F(\mathrm{x})$ denotes the crushing force at displacement x.

Subsequently, the SEA, which is an essential criterion for lightweight design, represents the energy absorbed per unit mass and can be defined as:

$$\mathrm{SEA} = \frac{\mathrm{EA}}{M} \tag{2}$$

where M is the total mass of the tube.

MCF is the mean crushing force, which is calculated as follows:

$$\mathrm{MCF} = \frac{\mathrm{EA}}{\mathrm{d}} \tag{3}$$

3 Finite Element Modeling

3.1 Specimen Preparation and Material Description

This paper investigated TTRST with different thickness distributions subjected to bending impact. According to previous research [6], the same thickness is assigned to the opposite side plates of the TTRST to keep the tube's symmetry. The cross sections of the baseline TTRST and the TTRST with different wall thicknesses are graphed in Fig. 1. In the side thickness model, the side plate thickness of the whole TTRST is changed, while the web plate thickness is changed in the web thickness model, as displaced in Fig. 1b and c. Aluminum alloy AA 6060 was adopted for the TTRST with various thicknesses. The mechanical properties of the material can be described in Table 1.

3.2 Finite Element Model

LS-Dyna, a nonlinear finite element code, was utilized to establish the finite element model of TTRSTs that were subjected to a three-point bending test, as shown in Fig. 2. The diameter of the cylindrical impactor and supports is 50 mm, and the span between the supports is 430 mm. A 128 kg impactor hit the TTRST with an initial velocity of 10 m/s. Automatic single-surface and automatic surface-to-surface contact were employed to simulate the self-contact of the TTRSTs and the contacts between the TTRSTs and the impactor or supports [6]. Further, the static and dynamic friction coefficients between the TTRST and the punch or supports were 0.2. The TTRST material AA6060 was modeled by mat 24 in LS-DYNA [50]. The rate-dependent effect was omitted in the FE model of the insensitivity of aluminum to strain rate at low impact velocities [51].

A convergence analysis was proposed to investigate the influence of mesh size on accuracy and find the optimum mesh size for the numerical models. Element sizes from 1.8 × 1.8 mm^2 to 4.0 × 4.0 mm^2 were selected based on the previous research [50]. The energy absorption of the TTRSTs with various element sizes was plotted in Fig. 2b. From Fig. 2b, there was a minor difference when the element sizes changed from 2.0 × 2.0 mm^2 to 1.8 × 1.8 mm^2, while the computational cost increased 53.85%. Thus, a finite element model

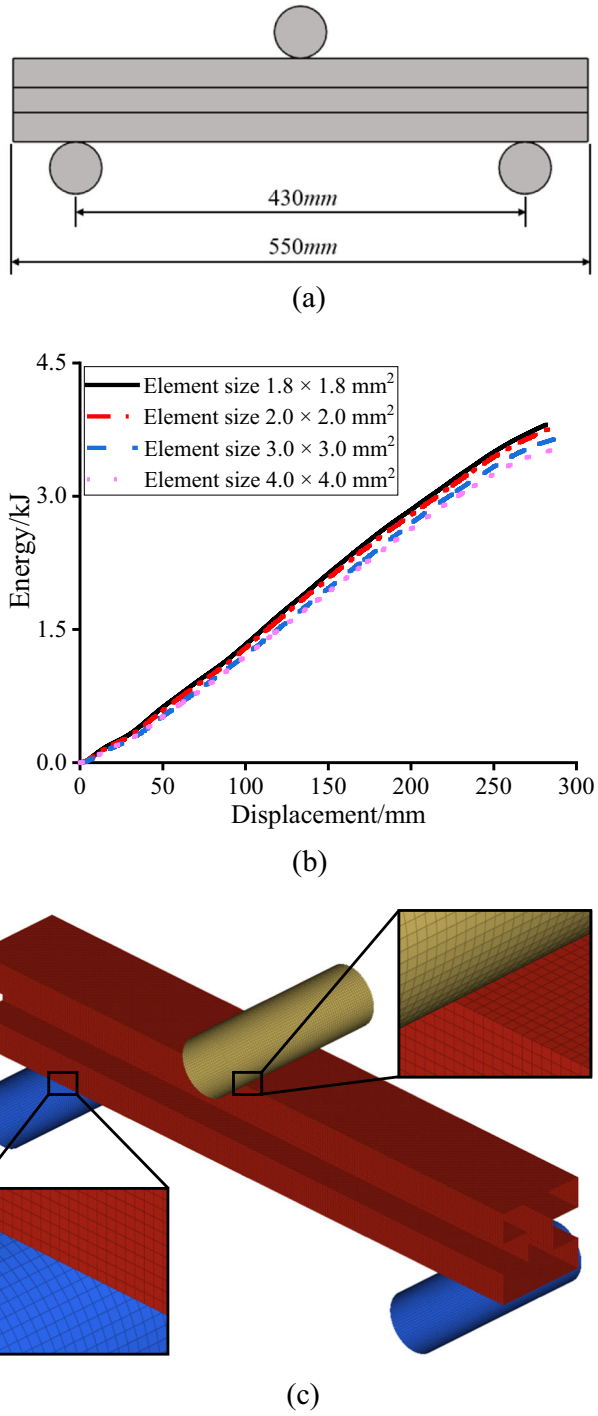

Fig. 2 **a** Geometrical configuration of the TTRST tube and its impact condition TTRST; **b** Convergence analysis of mesh size; **c** Finite element of TTRST

Table 1 The mechanical properties of the AA6060 [48, 49]

Density	Young's modulus	Initial yield stress	Poisson's ratio	Tangential modulus of elasticity
2.7×10^3 kg/m^3	68.566 GPa	227 MPa	0.29	321 MPa

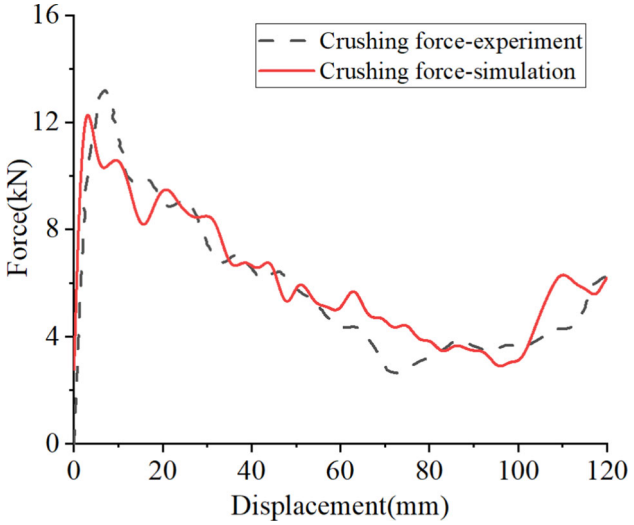

Fig. 3 Comparison of crushing force versus displacement of the TTRST between experiment [48] and simulation

with minor element sizes would not present a significant difference trend, while the computational cost could be highly increased. As a result, the Belytschko-Lin-Tsay thin shell elements with 2.0×2.0 mm^2 element size were adopted to build the FE models, as shown in Fig. 2c.

3.3 Validation of the FE Model

It should be noted that the TTRST would become square tubes when the corner number equaled four. Consequently, the FE model could be validated using a square tube constructed by previous research [48]. Figure 3 depicts the contrast between the experimental and finite element numerical results. The results reveal that the simulation's force versus displacement curves could accurately capture the tendency of the experiment curve. Therefore, the FE model is accurate and could provide considerable confidence in exploring the crashworthiness characteristic of TTRST.

4 Results and Discussions

4.1 Effect of Thickness

Previous research has conducted that thickness has a decisive influence on the energy absorption characteristic [21, 52–55]. As a result, the thickness is a crucial geometric factor that significantly influences the energy absorption performance of the TTRSTs. The energy absorption characteristics of a collection of TTRSTs with different thickness distributions in side plates (t_x) and web plate (t_y), respectively, were explored in the present work, as shown in Fig. 1b and c. These thickness distributions were set to 1.0 mm, 1.2 mm, 1.4 mm, 1.6 mm, 1.8 mm, 2.0 mm, 2.2 mm, 2.4 mm, 2.6 mm, 2.8 mm, and 3.0 mm. It should be emphasized that the weight of TTRSTs increased as their thickness increased, directly affecting the SEA.

The deformation patterns and energy absorption performance of the specimens are analyzed here. Huang and Zhang [56] conducted a series of experiments and found that tubes subjected to bending load usually demonstrated B, and I deformed mode, as shown in Fig. 4a and b. The top plate buckles in the middle in the B-mode, while the punch indents into the tube, and the bottom plate moves downward in the I mode. The stress and strain of the two typical deformed modes are depicted in Fig. 4c-f. The stress of the TTRST tube demonstrates that B-mode deformation is localized in the central narrow region of the top plate, as shown in Fig. 4. Conversely, the stress of the TTRST tube illustrates I mode deformation is concentrated near the edge of the top plate. Moreover, on the two TTRST plates, these two stress concentration regions likewise exhibit the most significant strain.

The deformation of the TTRSTs demonstrates a strong correlation between the deformation patterns and the wall thickness, as graphed in Fig. 5. Previous research [24, 57] illustrated that the more substantial flange resulted in higher bending strength, hampering the inward collapse of the top plates. As a result, when the thickness of the side wall of the TTRST tube is close to or greater than the thickness of the top, the TTRST tube exhibits B-mode deformation. In addition, as the thickness of the TTRST tube increases, the stress distribution of the TTRST tube undergoes a change process from concentrated to uniform and then uniform to concentrated.

Additionally, the support was more considerable when the distinctive edge and center structure of the TTRST (as illustrated in Fig. 6a) were thicker. The TTRST cavity collected this distinctive structure when the TTRST was bent. Moreover, when the side plate and web plate thickness increased, so did the bulge of the flange located at the bottom of the TTRST, resulting in the flange deviating further outward, as illustrated in Fig. 6b and c. Furthermore, when t_x ort_y was

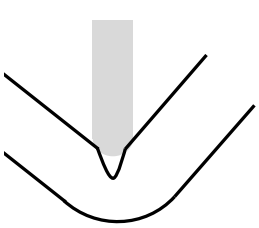

(a) Bending collapse (B mode)

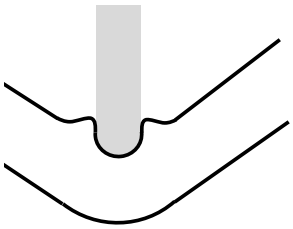

(b) Bending with Indentation (I mode)

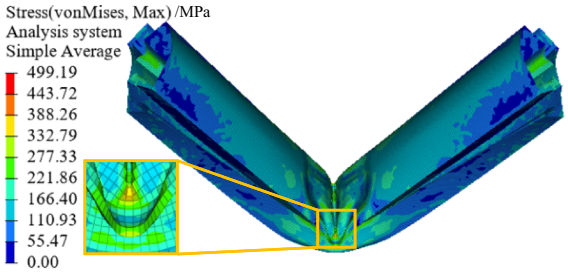

(c) Stress of TTRST with B mode deformation

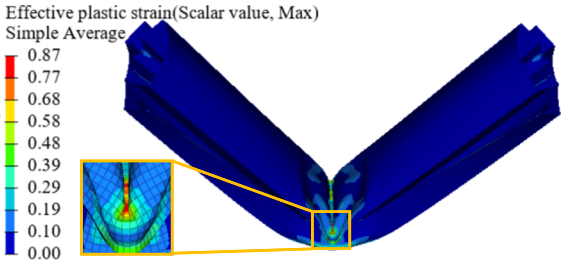

(d) Strain of TTRST with B mode deformation

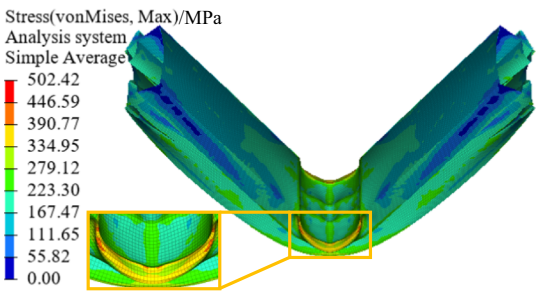

(e) Stress of TTRST with I mode deformation

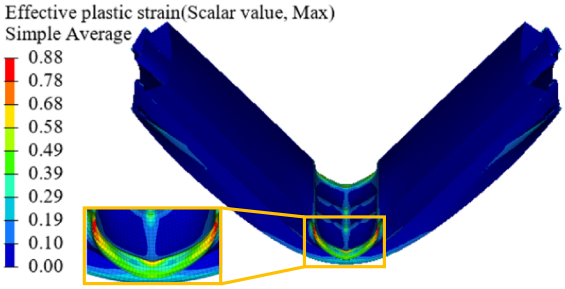

(f) Strain of TTRST with I mode deformation

Fig. 4 Typical deformation modes of thin-walled tubes

greater than 1.4 mm, the edge and middle of the bottom flange produced noticeable protrusion, as shown in Fig. 5.

Figure 7 depicts the relationship between IPF and MCF versus the different thicknesses of the TTRSTs. It can be seen from Fig. 7 that the IPF and MCF of TTRSTs presented a general upward trend with thickness increase, indicating that thickness has a decisive influence on the crushing force curve.

Further, in the side plate cases, the crushing force curve (including IPF and MCF) presented a larger slope when the side plate thickness was in the region of $t_x \in [1.0, 1.8)$ than in the other regions. Consequently, IPF and MCF were more sensitive to the side plate thickness in this region. For a TTRST with $t_x \in [1.0, 2.0)$, the side plate was thinner than the web plate. Such a thin side plate could not limit the TTRST bent deformation of the tube in the early stage and improve the tube's deformation's effectiveness in decreasing the impact force, resulting in a smaller IPF and MCF.

In the web plate cases, the IPF of the TTRSTs prescribed a similar trend as that of the side plate cases. However, the MCF of the web plate increased in the region of $t_y \in [1.0, 2.6]$ and decreased for $t_y \in [2.6, 2.8]$, which was different from the side plate cases. Besides, the IPF of the web plate cases was lower than that of the side plate case in the thickness $T <$ 2.0 mm, while the MCF of the web plate case was lower than that of the side plate cases in the thickness $T > 2.2$ mm. This discovery is beneficial since optimizing the wall thickness can enhance the TTRSTs' energy absorption properties.

The relationships of SEA regarding thicknesses are shown in Fig. 8. The TTRSTs' bending was effectively restricted by the thickness increase, resulting in the tubes retaining an asymptotically stable deformation mode with significant energy absorption. However, the TTRSTs' increased mass due to their rising thickness significantly affected their SEA. Hence, the result in Fig. 8 showed that the SEA of TTRSTs exhibited oscillatory rise.

In the side plate case, the TTRSTs' SEA also reduced with increasing thickness in the $t_x \in$ [1.0, 1.2] U [1.8, 2.0] U [2.4, 3.0], whereas it increased with increasing thickness in the $t_x \in$ [1.2, 1.8] U [2.0, 2.4]. Additionally, compared to

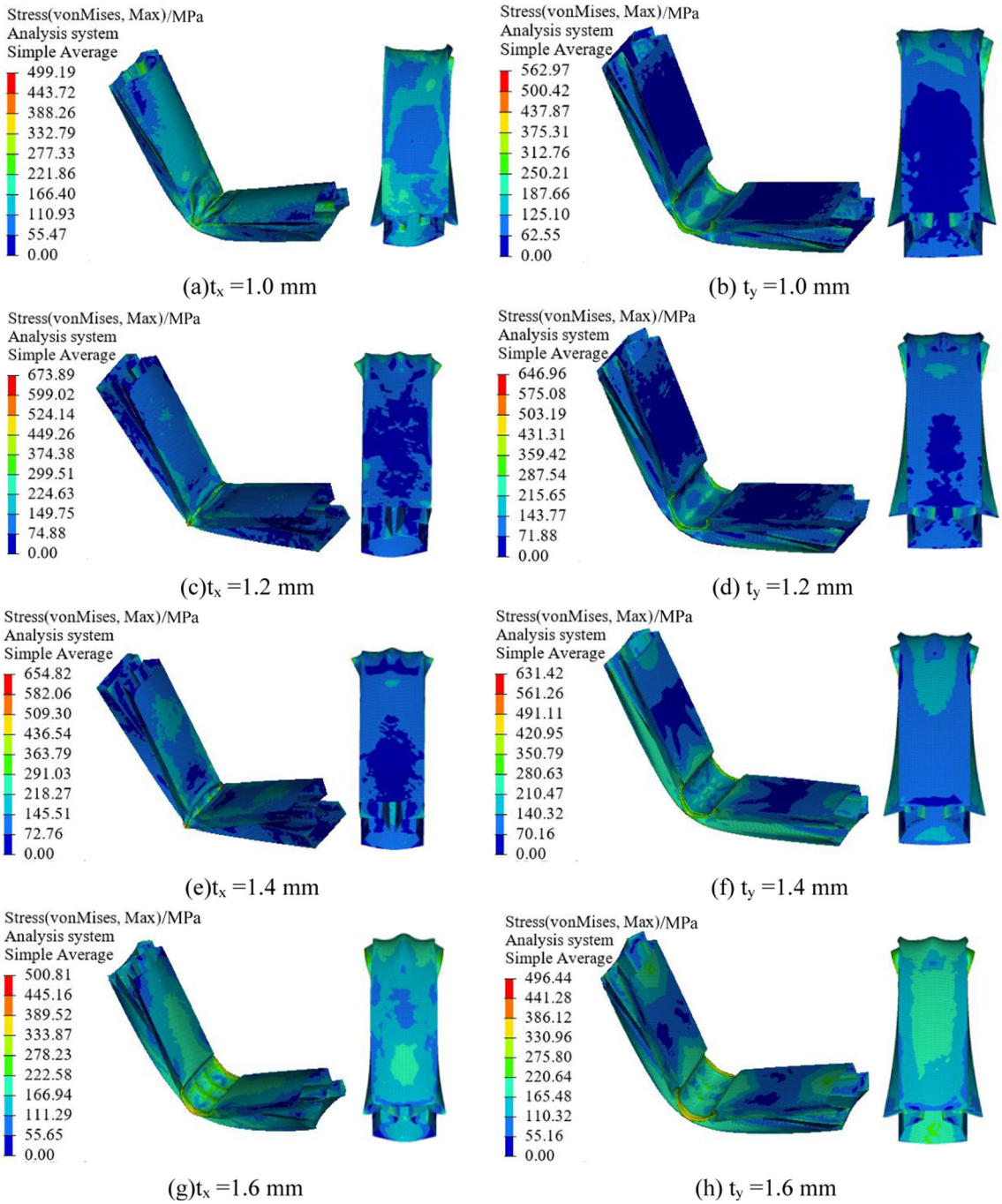

Fig. 5 Deformation patterns of TTRSTs with different

other regions, the SEA curve exhibited a higher change rate in the side plate thickness range from 1.2 mm to 1.6 mm. In other words, the thickness in the $t_x \in [1.2, 1.6]$ strongly influenced the SEA. Besides, the SEA for the web plate case was generally lower than that of the side plate case in most situations (6 of 11 thickness points). Moreover, in the side plate and web plate thickness cases, the SEA reached its maximum value when thickness (including side plate and web plate thickness) was close to 2.5 mm, indicating a more significant effective energy absorption.

4.2 Effects of the Impact Position

The impactor hitting the side plate or web plate could present a different energy absorption characteristic since the two adjacent plates of the TTRST exhibit different shapes.

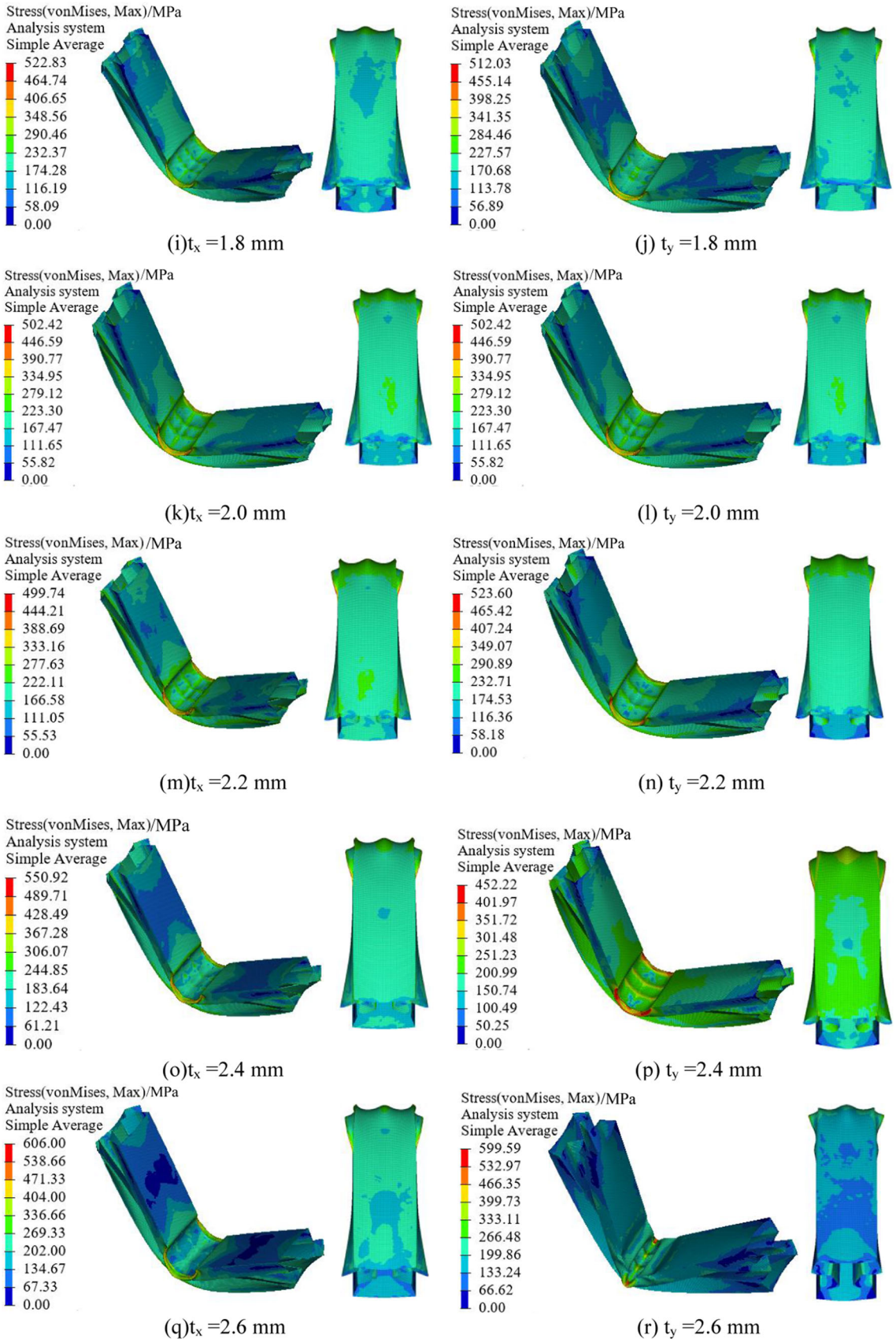

Fig. 5 continued

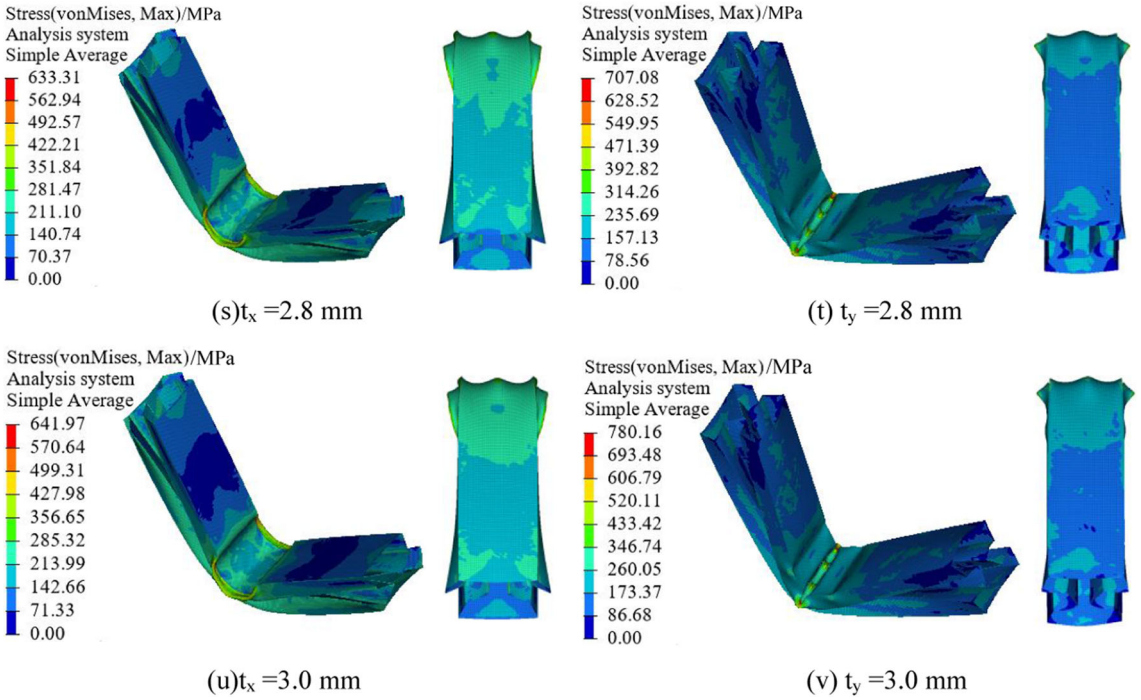

Fig. 5 continued

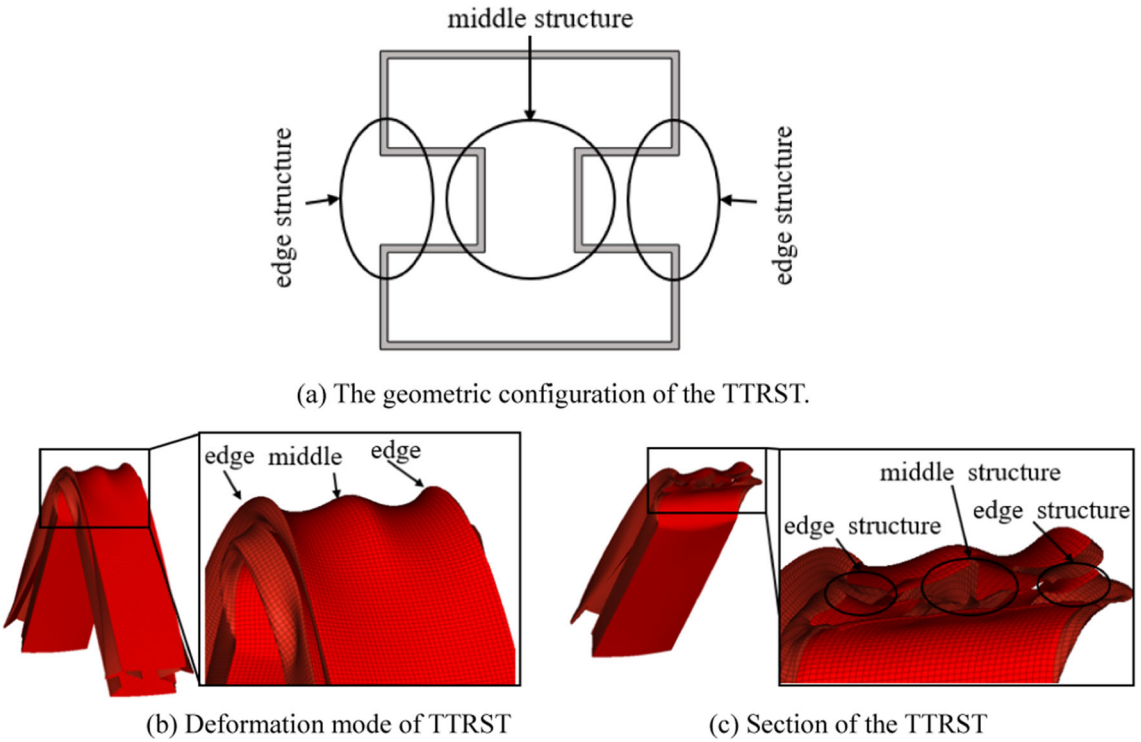

Fig. 6 An illustration of deformation for TTRST with thicker side support

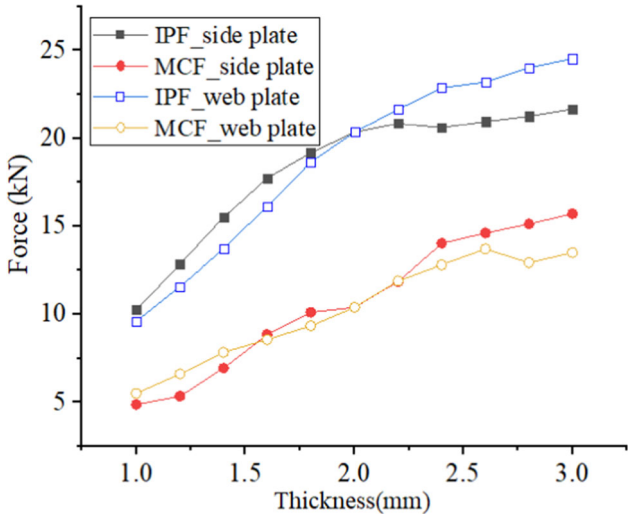

Fig. 7 IPF and MCF versus thickness

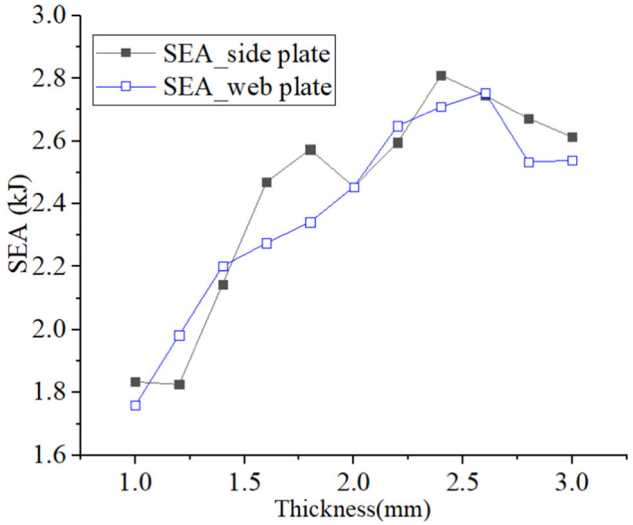

Fig. 8 SEA versus thickness

Therefore, it is worth investigating the energy absorption performance of the TTRSTs subjected to web plate impact to understand the TTRSTs' energy absorption performance further while the impactor hit the side plate situation has been proposed, as shown in Fig. 9.

The deformed shapes of TTRSTs subjected to web plate impact are graphed in Fig. 10. The deformation modes of side plate thickness cases and web plate thickness cases were similar in the web plate impact situation. In addition, all the TTRSTs subjected to model B impact position presented B deformation mode. Furthermore, as the thickness increased, the TTRST tube's stress distribution became more uniform.

For side plate cases, the thicker side plate thickness retarded the formation of the inward fold of the top plate and reduced the displacement of the impactor invading TTRST. Besides, when the thickness of the side plate was less than 1.8 mm, the side plate lacked sufficient support and collapsed outward during the bending process, as shown in Fig. 10a. For the web plate cases, as the thickness of the web plate increased, the inward depression of the top panel decreased slightly, and this decreasing trend was consistent with that of the side plate cases.

As illustrated in Fig. 11a, the IPF of those four situations all presented a general upward trend. Besides, the IPF of model B (linked to Fig. 9b) with side plate thickness changing was lower than that of the model B with web plate thickness changing for thickness $T \in [1.0, 2.0]$, while the IPF of model B with side plate thickness changing was higher than that of the model B with web plate thickness changing for $T \in [2.0, 3.0]$. Further, the two model B cases (side plate and web plate thickness) illustrated a higher IPF than the two model A cases (linked to Fig. 9a). Therefore, a suitable thickness could be employed to improve the energy absorption characteristic of the TTRSTs that need to be optimized.

The SEA of TTRSTs subjected to model A impact was lower than that of model B impact at the same thickness. Moreover, the SEA reached its maximum value in all four situations when the TTRST's thickness was close to 2.4 mm, indicating that a more significant effective energy absorption could be reached when the thickness of the TTRSRT was close to 2.4 mm. Additionally, as shown in Fig. 11c, similar to the changing trend of the IPF curve, the MCF of model A and model B generally increased with the increased thickness. At the same time, model B's MCF was higher than model A's under the same thickness condition.

Fig. 9 Impact condition of TTRSTs

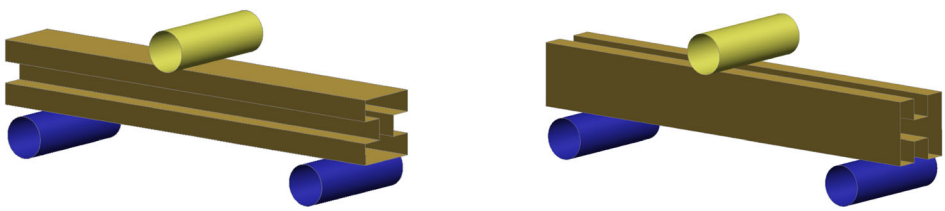

(a) Impactor hit side plate (Model A) (b) Impactor hit web plate (Model B)

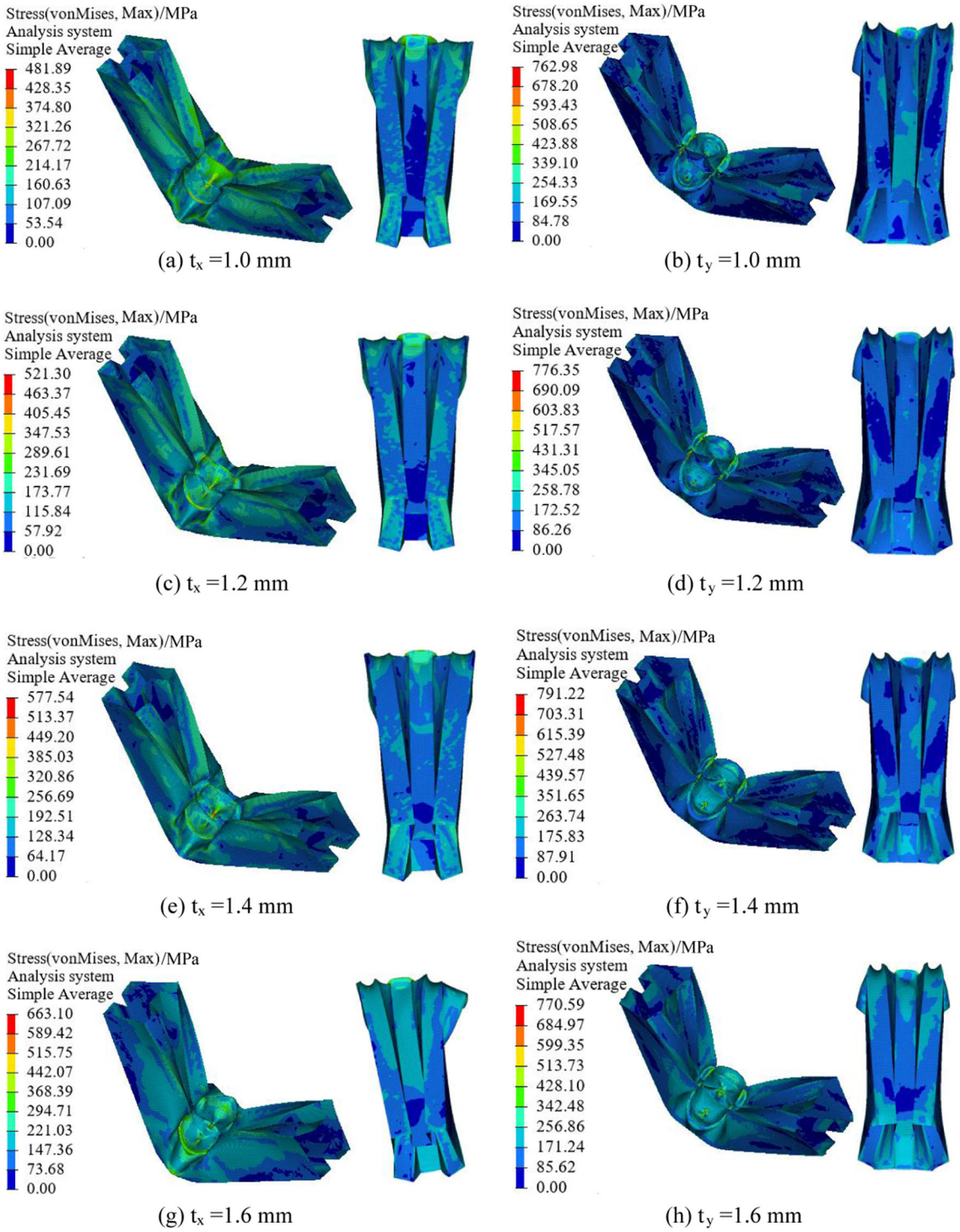

Fig. 10 Deformation patterns of TTRSTs with different thicknesses (Model B)

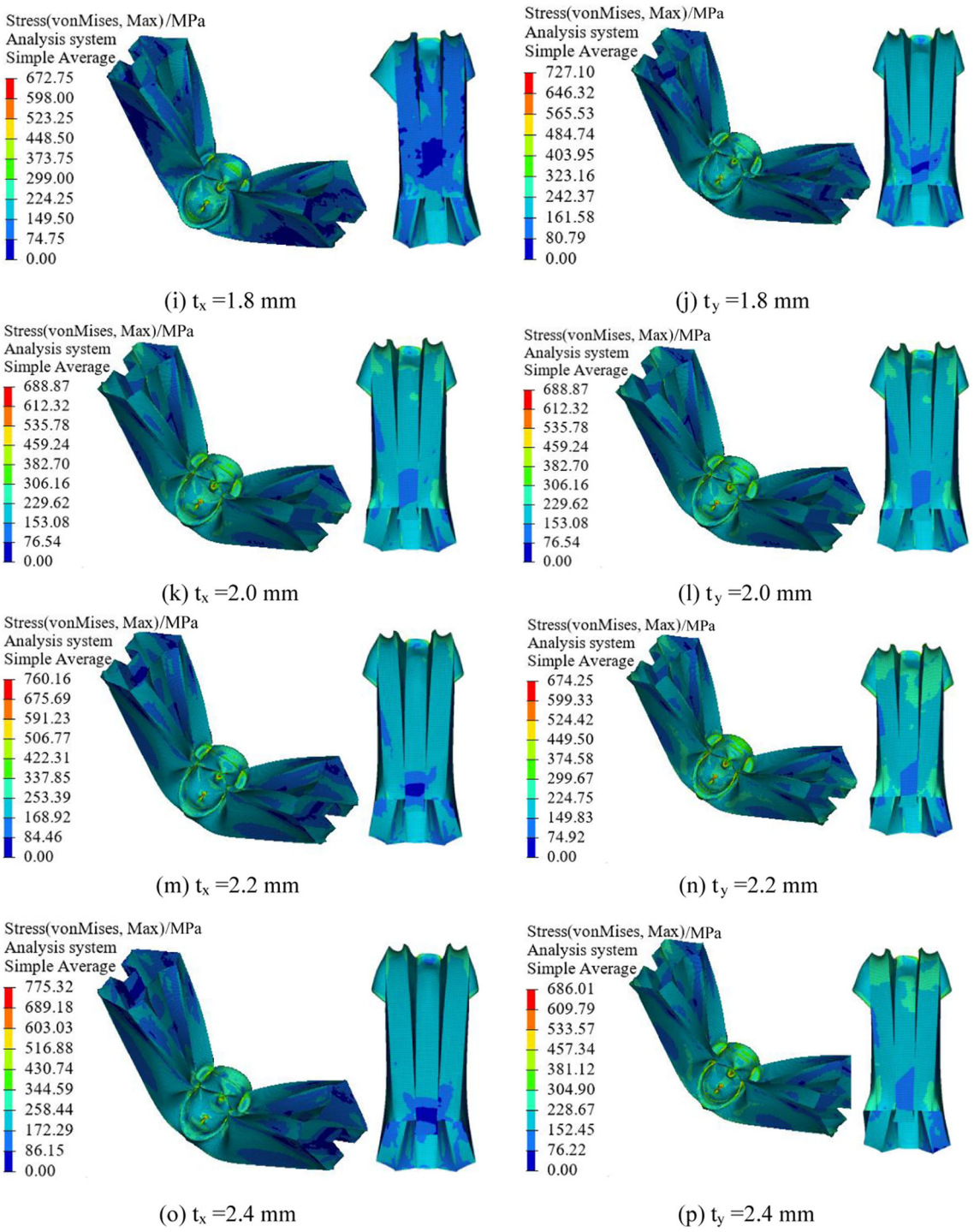

Fig. 10 continued

4.3 Energy Absorption Characteristic Optimization

A multiobjective energy absorption optimization method was adopted to improve further TTRST's energy absorption performance, in which the Opt LHD (Optimal Latin hypercube design) method and RSM (Response surface methodology) were used to erect approximation models. In the principle of Opt LHD, experimental factors are divided into multiple levels and arranged as evenly as possible in the experimental design. Each level is evenly distributed throughout the experimental design to ensure that each level has the same

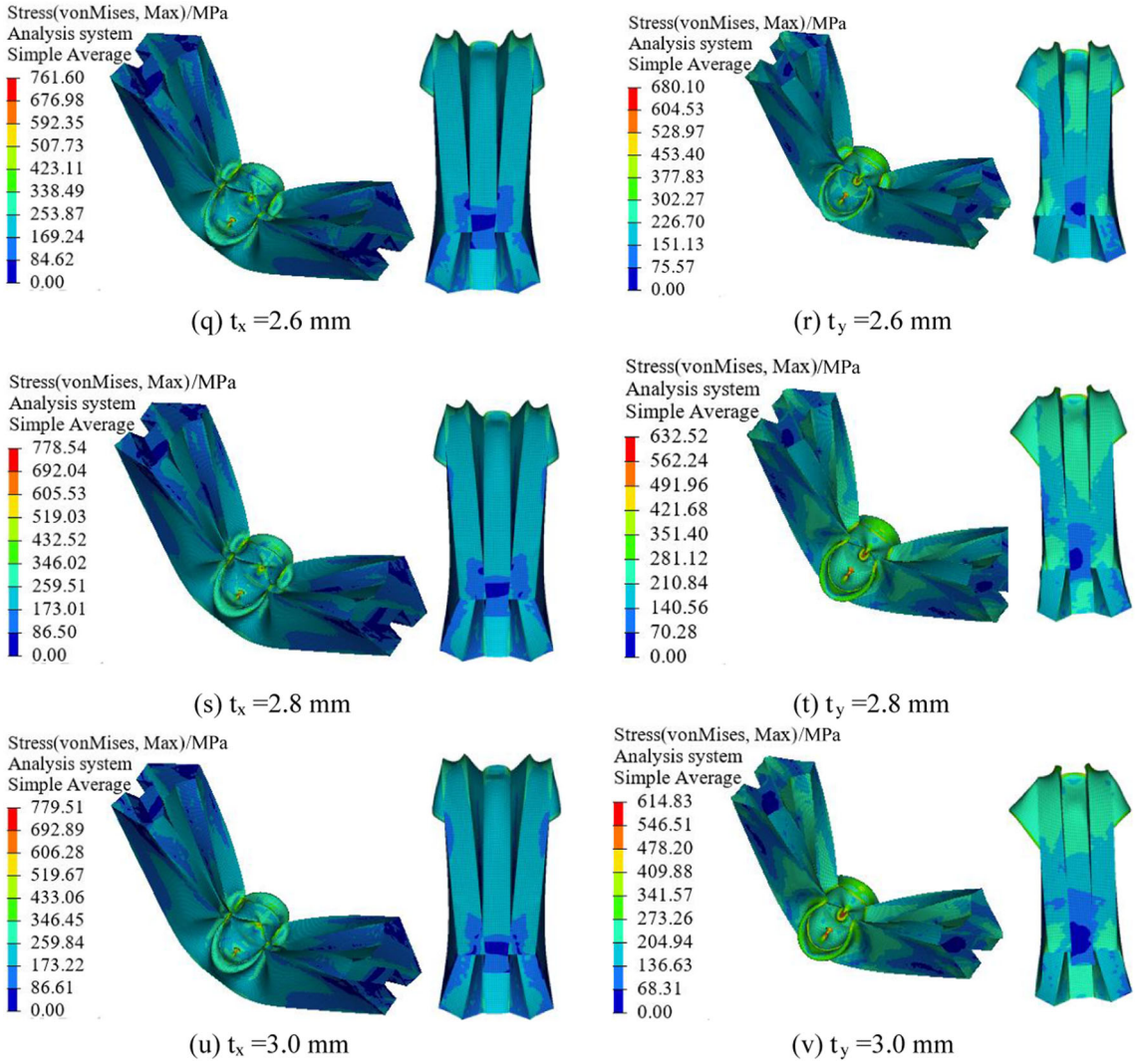

Fig. 10 continued

number of occurrences. Hence, Opt LHD can avoid significant bias in the experimental results due to the influence of a certain level. Besides, the basic principle of RSM is to use polynomial functions to fit the design space. Lai et al. [58] illustrated that the relationship between the minimum number of samples and the number of input variables for constructing a fourth-order polynomial RSM is:

$$N = \frac{(M+1)(M+2)}{2} + 2M \tag{4}$$

where N is the minimum number of samples, M denotes the number of input variables.

According to experience, when the number of sample points is 2–5 times the minimum number, it will have a better polynomial fitting effect and prevent many samples from consuming too much time. Hence, the Opt LHD method was employed to create 50 sets of experiments in this study.

In addition, genetic algorithms have been widely utilized to find succeeding particles using natural evolution methods [59, 60]. As a result, NSGA-II (Non-Dominated Sorting Genetic Algorithm-II), with good exploratory ability in non-dominated sorting, was utilized as a multiobjective optimization method herein. The layout of the genetic algorithm-based optimization method was plotted in Fig. 12.

Figure 13 prescribes the IPF, SEA, and MCF of the 50 simulations. As shown in Fig. 12, RSM was utilized to fit the relationship between input variables and output variables through polynomial functions. The functional connection between the IPF (Y_1), SAE (Y_2), MCF (Y_3), and the side plate thickness (t_x) and web plate thickness (t_y) was presented in Eqs. (5)–(10). Besides, their average and root mean square errors were within the acceptable range, as shown in Table 2. As a result, those approximation models provided a good prediction effect and could be utilized in multiobjective

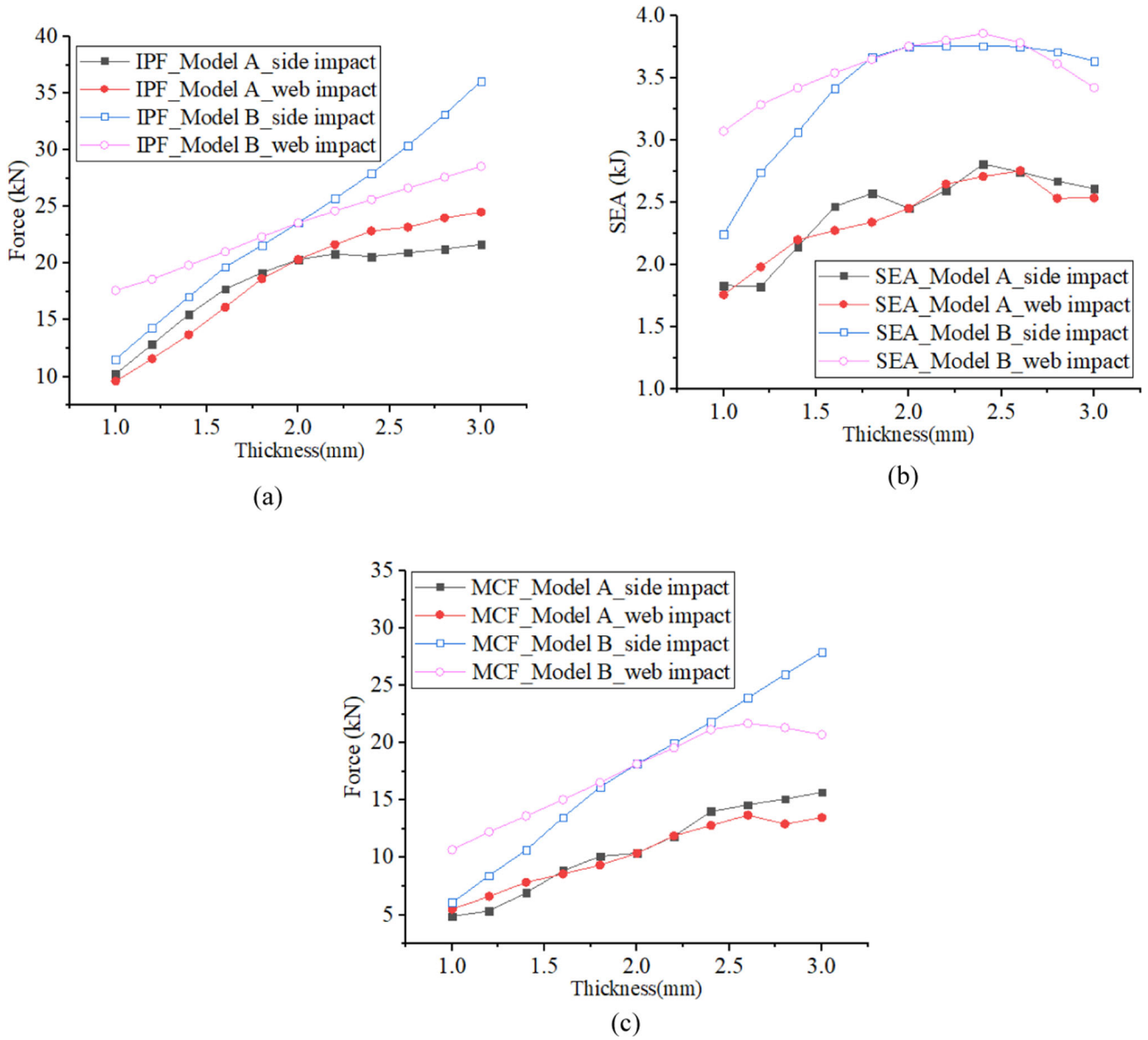

Fig. 11 Comparison of energy-absorbed characteristics of TTRSTs with different thicknesses. **a** IPF; **b** SEA; **c** MCF

optimization.

$$Y_{1\_side\_plate\_impact} = 2.5867 + 3.0430t_x t_y - 0.4211t_x^2 \quad (5)$$

$$Y_{2\_side\_plate\_impact} = 1.5932 + 0.6008t_x t_y - 0.0770t_x^3 - 0.0681t_y^3 \quad (6)$$

$$Y_{3\_side\_plate\_impact} = 1.7516 + 4.9599t_x t_y - 1.1014t_x^2 - 1.2518t_y^2 \quad (7)$$

$$Y_{1\_web\_plate\_impact} = -1.3851 + 9.3024t_x + 1.8451t_x t_y \quad (8)$$

$$Y_{2\_web\_plate\_impact} = -0.7762 + 3.7698t_x + 0.2836t_x t_y - 0.9448t_x^2 - 0.0147t_y^4 \quad (9)$$

$$Y_{3\_web\_plate\_impact} = 1.3777 + 6.3558t_x t_y - 1.7799t_y^2 - 0.1054t_x^3 \quad (10)$$

The optimum TTRST with the lowest IPF and the highest SEA and MCF was determined using a multiobjective crashworthiness optimization based on the NSGA-II. This was shown by the equations in Eq. (11).

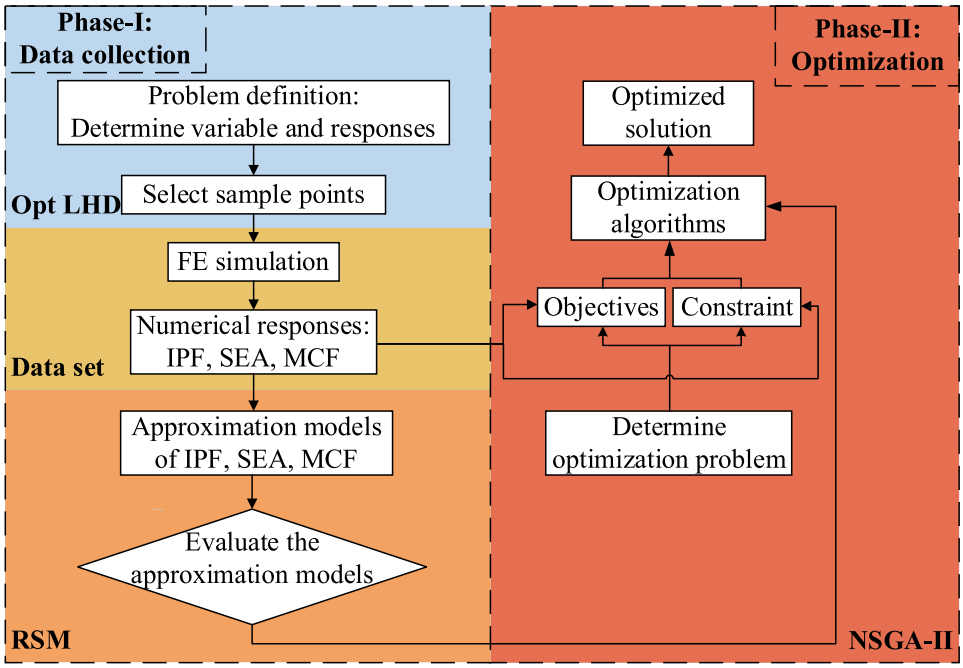

Fig. 12 The flowchart of the optimization

$$\begin{cases} \text{Min(IPF, - SEA, - MCF)} \\ \text{s.t.} \begin{cases} 1\ \text{mm} \le t_x \le 3\ \text{mm} \\ 1\ \text{mm} \le t_y \le 3\ \text{mm} \end{cases} \end{cases} \tag{11}$$

According to previous research [61], Fig. 14a graphed a new Pareto front as solid balls in which the optimal design ($t_x = 2.47$ mm, $t_y = 1.84$ mm) subjected to the constraint IPF $\le$ 14 kN masked as a red ball, while Fig. 14b depicted the Pareto front of TTRSTs subjected to web plate impact with the optimal design ($t_x = 1.11$ mm, $t_y = 2.07$ mm) masked as a red ball. Further, the differences between the optimal TTRST and baseline TTRST ($t_x = 2.0$ mm, $t_y = 2.0$ mm) were listed in Table 3. The results of Table 2 indicated that the value of IPF does not violate the constraint. Furthermore, the change of IPF, SEA, and MCF subjected to side plate impact was 4.60%, −8.36%, and 2.61%, respectively, while the change of IPF, SEA, and MCF subjected to web plate impact was −46.92%, −34.01%, and −58.32%, respectively. On the one hand, the optimal results illustrated a lower SEA, as TTRSTs introduced in this paper present the highest SEA when the wall's thickness is near 2.5 mm. On the other hand, the results shown that choosing a reasonable thickness can reduce IPF by 46.92% or increase MCF by 2.61%, thereby improving the energy absorption characteristics of TTRST.

5 Conclusion

This study proposed the TTRSTs to investigate their energy absorption characteristics under bending impact. The configurations controlled by the side plate and web plate thickness significantly affected the TTRSTs' energy absorption characteristic subjected to the impact of the side plate and web plate. Conclusions can be drawn as follows:

(1) The deformation modes of the TTRSTs could substantially affect the side plate or web plate thicknesses. As the thickness increases, the middle part of the bottom plate bulges outward more seriously during the bending process.
(2) In the side plate impact, IPF and MCF showed an increasing trend with the increase in thickness, while SEA showed a trend of first increasing and then decreasing. Besides, the TTRST has a maximum SEA when the thickness (side plates and web plates) is around 2.4 mm.
(3) In the web plate impact, IPF, SEA, and MCF show similar variation trends to the side plate impact. It should be noted that the IPF, SEA, and MCF in the web plate impact are larger than those in the side plate impact at the same thickness. Further, it implied that a suitable thickness results in a good energy absorption characteristic.

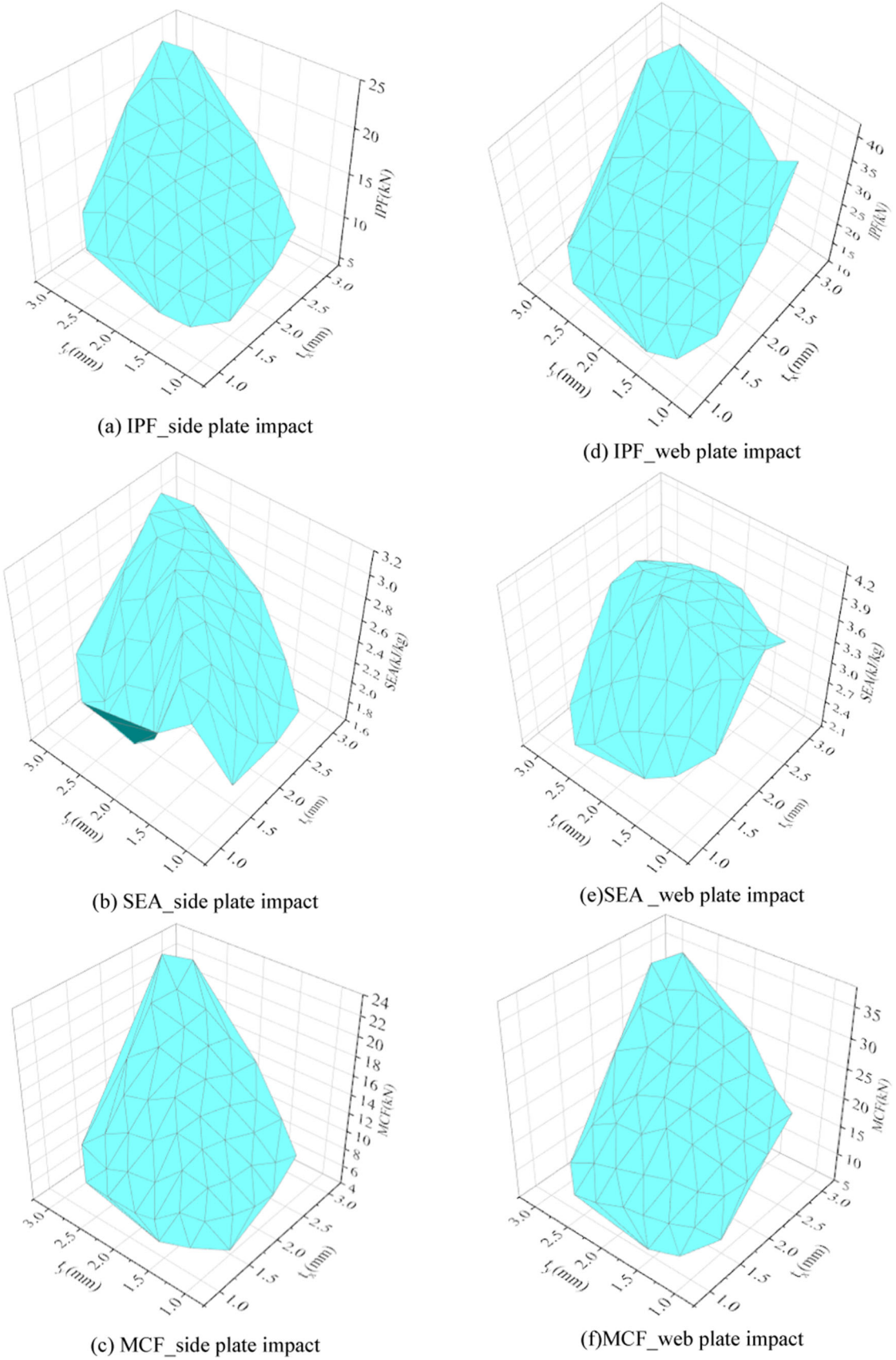

(a) IPF_side plate impact

(d) IPF_web plate impact

(b) SEA_side plate impact

(e)SEA _web plate impact

(c) MCF_side plate impact

(f)MCF_web plate impact

Fig. 13 Energy-absorbed characteristics of TTRST tubes

Table 2 Accuracies of the approximation models

Error type	Side plate impact			Web plate impact			Acceptan level
	IPF	SEA	MCF	IPF	SEA	MCF	
Average	0.02	0.12	0.04	0.02	0.05	0.03	0.2
Root mean square	0.03	0.15	0.05	0.04	0.07	0.03	0.2

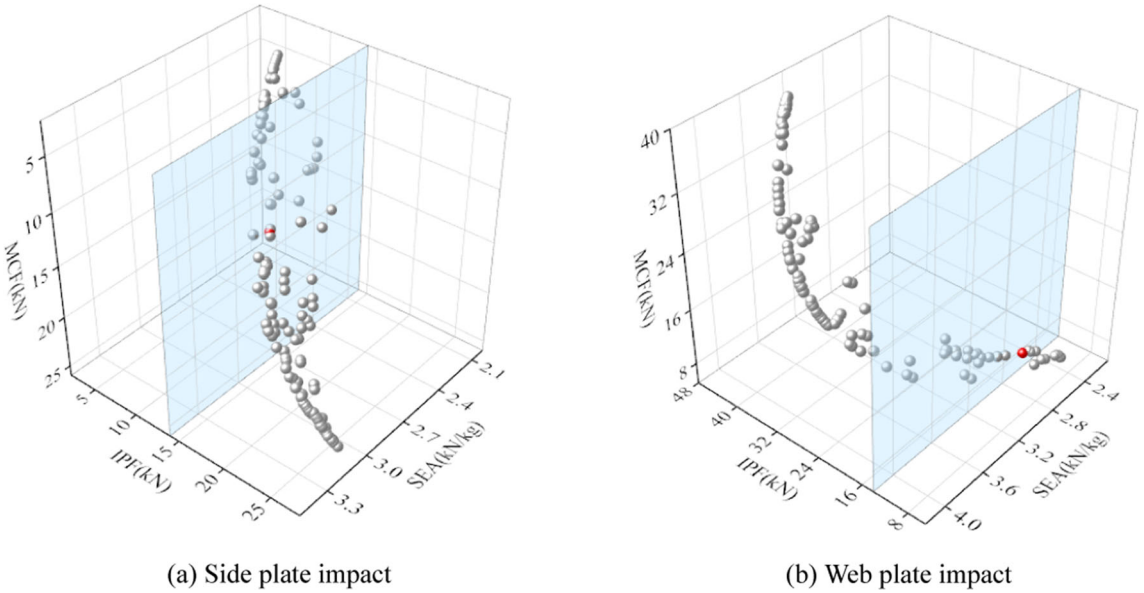

Fig. 14 Pareto front of TTRSTs

Table 3 Comparison of optimal design results of optimal and baseline

	Side plate impact			Web plate impact		
	IPF (kN)	SEA (kJ/kg)	MCF (kN)	IPF (kN)	SEA (kJ/kg)	MCF (kN)
Baseline	13.27	2.99	13.03	24.83	3.97	19.70
Optimal	13.88	2.74	13.37	13.18	2.62	8.21
Change	4.60%	−8.36%	2.61%	−46.92%	−34.01%	−58.32%

6 Future Work

Since the TTRST structure proposed herein could theoretically be manufactured by rolling, laser welding, and other processes, TTRST also has welding difficulties. Besides, local stress concentration occurred in the middle part of the TTRST tube during the three-point bending experiment because the hollow TTRST tube does not provide sufficient resistance to deformation. Furthermore, foam-filled tubes have better bending resistance than hollow tubes. As a result, a new type of foam-filled TTRST fabricated by folding metal sheets will be investigated.

Acknowledgements This paper is supported by the Special project of Chongqing Banan District Science and Technology Bureau: "Structural lightweight design technology of car body front longitudinal beam", the Chongqing Science and Technology Innovation and Application Development Special Key Project (cstc2021jscx-cy1hX0006) and the 2022 Guangxi University Young and Middle-aged Teachers' Basic Research Ability Improvement Project (Grant No. 2022KY0781).

Funding Structural lightweight design technology of car body front longitudinal beam, Chongqing Science and Technology Innovation and Application Development Special Key Project (cstc2021jscx-cy1hX0006), 2022 Guangxi University Young and Middle-aged Teachers' Basic Research Ability Improvement Project (Grant No. 2022KY0781).

Declarations

Competing interest The authors declare that they have no known competing financial interests or personal relationships that could have appeared to influence the work reported in this paper.

References

1. Sun, G.; Tian, X.; Fang, J.; Xu, F.; Li, G.; Huang, X.: Dynamical bending analysis and optimization design for functionally graded thickness (FGT) tube. Int. J. Impact Eng **78**, 128–137 (2015)
2. Liu, X.; Liang, R.; Hu, Y.; Tang, X.; Bastien, C.; Zhang, R.: Collaborative optimization of vehicle crashworthiness under frontal impacts based on displacement oriented structure. Int. J. Automot. Technol. **22**(5), 1319–1335 (2021)
3. Lu, G.; Yu, T.: Energy Absorption of Structures and Materials. CRC Press;Woodhead Publishing, Boca Raton, Cambridge (2003)
4. Duan, L.; Du, Z.; Jiang, H.; Xu, W.; Li, Z.: Theoretical prediction and crashworthiness optimization of top-hat thin-walled structures under transverse loading. Thin-Walled Struct. **144**, 10621 (2019)
5. Rincón-Dávila, D.; Alcalá, E.; Martín, Á.: Theoretical–experimental study of the bending behavior of thin-walled rectangular tubes. Thin-Walled Struct. **173**, 109009 (2022)
6. Zhang, X.; Zhang, H.; Wang, Z.: Bending collapse of square tubes with variable thickness. Int. J. Mech. Sci. **106**, 107–116 (2016)
7. Liang, R.; Liu, N.; Liu, X.; Wei, T.; Mo, L.; Huang, H., et al.: Energy absorption performance of bionic multi-cell tubes inspired by shrimp chela. Acta Mech. Solida Sin. **36**(5), 754–762 (2023)
8. Su, M.; Wang, H.; Hao, H.: Axial and radial compressive properties of alumina-aluminum matrix syntactic foam filled thin-walled tubes. Compos. Struct. **226**, 111197 (2019)
9. Wang, Q.; Fan, Z.; Gui, L.: Theoretical analysis for axial crushing behaviour of aluminium foam-filled hat sections. Int. J. Mech. Sci. **49**(4), 515–521 (2007)
10. Abramowicz, W.; Wierzbicki, T.: Axial crushing of multicorner sheet metal columns. J. Appl. Mech. Trans. Asme **56**, 113–120 (1989)
11. Liang, R.; Liu, X.; Hu, Y.; Jiang, C.; Bastien, C.: A methodology to investigate and optimise the crashworthiness response of foam-filled twelve right angles thin-walled structures under axial impact. Compos. Struct. **310**, 116736 (2023)
12. Li, S.; Guo, X.; Li, Q.; Ruan, D.; Sun, G.: On lateral compression of circular aluminum CFRP and GFRP tubes. Compos. Struct. **232**, 111534 (2020)
13. Liu, Q.; Xu, X.; Ma, J.; Wang, J.; Shi, Y.; Hui, D.: Lateral crushing and bending responses of CFRP square tube filled with aluminum honeycomb. Compos. B Eng. **118**, 104–115 (2017)
14. Tran, T.N.; Ton, T.N.T.: Lateral crushing behaviour and theoretical prediction of thin-walled rectangular and square tubes. Compos. Struct. **154**, 374–384 (2016)
15. Xiong, G.; Feng, Y.; Liao, X.-D.; Gu, Y.; Kang, S.-B.: Lateral—torsional buckling behaviour of welded Q690 steel I-beams with double lateral restraints along the length. Thin-Walled Struct. **170**, 108659 (2022)
16. Zhang, X.; Zhang, H.; Ren, W.: Bending collapse of folded tubes. Int. J. Mech. Sci. **117**, 67–78 (2016)
17. Zhang, X.; Zhang, H.: Static and dynamic bending collapse of thin-walled square beams with tube filler. Int. J. Impact Eng. **112**, 165–179 (2018)
18. Lavayen-Farfan, D.; Boada, M.J.L.; Rodriguez-Hernandez, J.A.: Bending collapse analysis for thin and medium-thin-walled square and rectangular hollow shapes. Thin-Walled Struct. **165**, 107934 (2021)
19. Xu, F.; Tian, X.; Li, G.: Experimental study on crashworthiness of functionally graded thickness thin-walled tubular structures. Exp. Mech. **55**(7), 1339–1352 (2015)
20. Yang, Y.-F.; Zhang, Z.-C.; Fu, F.: Experimental and numerical study on square RACFST members under lateral impact loading. J. Constr. Steel Res. **111**, 43–56 (2015)
21. Hanssen, A.G.; Hopperstad, O.S.; Langseth, M.: Bending of square aluminium extrusions with aluminium foam filler. Acta Mech. **142**, 13–31 (2000)
22. Zhang, H.; Zhang, X.; Fu, X.: Experimental and numerical investigations on three-point bending collapse of thin-walled beams. Eng. Struct. **293**, 116614 (2023)
23. Kecman, D.: Bending collapse of rectangular and square section tubes. Int. J. Mech. Sci. **25**(9), 623–636 (1983)
24. Lavayen-Farfan, D.; Butenegro-Garcia, J.A.; Boada, M.J.L.; Martinez-Casanova, M.A.; Rodriguez-Hernandez, J.A.: Theoretical and experimental study of the bending collapse of partially reinforced CFRP–Steel square tubes. Thin-Walled Struct. **177**, 109457 (2022)
25. Du, Z.; Duan, L.; Cheng, A.; Xu, Z.; Zhang, G.: Theoretical prediction and crashworthiness optimization of thin-walled structures with single-box multi-cell section under three-point bending loading. Int. J. Mech. Sci. **157–158**, 703–714 (2019)
26. Yin, H.; Wen, G.; Bai, Z.; Chen, Z.; Qing, Q.: Theoretical prediction and crashworthiness optimization of multi-cell polygonal tubes. J. Sandw. Struct. Mater. **22**, 190–219 (2017)
27. Liu, X.; Liang, R.; Hu, Y.; Jiang, C.; Tang, X.; Bastien, C.: Body optimization approach of sedan structure for improving small overlap impact rating. Int. J. Crashworthiness **26**(2), 182–190 (2021)
28. Zhang, X.; Zhang, H.; Leng, K.: Experimental and numerical investigation on bending collapse of embedded multi-cell tubes. Thin-Walled Struct. **127**, 728–740 (2018)
29. Huang, Z.; Zhang, X.; Yang, C.: Experimental and numerical studies on the bending collapse of multi-cell aluminum/CFRP hybrid tubes. Compos. B Eng. **181**, 107527 (2020)
30. Kim, H.-S.; Wierzbicki, T.: Numerical and analytical study on deep biaxial bending collapse of thin-walled beams. Int. J. Mech. Sci. **42**(10), 1947–1970 (2000)
31. Yıldız, B.; Mehta, P.; Sait, S.; Panagant, N.; Kumar, S.; Yildiz, A.: A new hybrid artificial hummingbird-simulated annealing algorithm to solve constrained mechanical engineering problems. Mater. Test. **64**, 1043–1050 (2022)
32. Yıldız, B.: Slime mould algorithm and kriging surrogate model-based approach for enhanced crashworthiness of electric vehicles. Int. J. Veh. Des. **83**, 54 (2020)
33. Aye, C.; Pholdee, N.; Bureerat, S.; Sait, S.; Yildiz, A.: Multi-surrogate-assisted metaheuristics for crashworthiness optimisation. Int. J. Veh. Des. **80**, 2019 (2020)
34. Liang, R.; Xu, F.; Zhu, Y.; Liu, X.; Mo, L.; Liu, N.: Dynamic response of bionic non-convex tubes with proportional distribution of bulkhead. Proc. Inst. Mech. Eng. Part C J. Mech. Eng. Sci. **45**, 456 (2023). https://doi.org/10.1177/09544062231204536
35. Sun, G.; Pang, T.; Zheng, G.; Song, J.; Li, Q.: On energy absorption of functionally graded tubes under transverse loading. Int. J. Mech. Sci. **115–116**, 465–480 (2016)
36. Fu, X.; Zhang, X.: Three-point bending of thin-walled arched beams with square sections. Thin-Walled Struct. **182**, 110201 (2023)
37. Wu, F.; Chen, Y.; Zhao, S.; Hong, Y.; Zhang, Z.; Zheng, S.: Mechanical properties and energy absorption of composite bio-inspired multi-cell tubes. Thin-Walled Struct. **184**, 110451 (2023)
38. Yildirim, A.; Demirci, E.; Karagöz, S.; Özcan, Ş; Yildiz, A.: Experimental and numerical investigation of crashworthiness performance for optimal automobile structures using response surface methodology and oppositional based learning differential evolution algorithm. Mater. Test. **65**, 346–363 (2023)
39. Zhang, H.; Sun, G.; Xiao, Z.; Li, G.; Li, Q.: Bending characteristics of top-hat structures through tailor rolled blank (TRB) process. Thin-Walled Struct. **123**, 420–440 (2018)

40. Sun, G.; Zhang, H.; Fang, J.; Li, G.; Li, Q.: Multi-objective and multi-case reliability-based design optimization for tailor rolled blank (TRB) structures. Struct. Multidiscip. Optim. **55**(5), 1899–1916 (2016)
41. Zhang, J.; Wu, L.; Chen, G.; Zhou, H.: Bending collapse theory of thin-walled twelve right-angle section beams. Thin-Walled Struct. **85**, 377–387 (2014)
42. Zhang, J.; Zhou, H.; Wu, L.; Chen, G.: Bending collapse theory of thin-walled twelve right-angle section beams filled with aluminum foam. Thin-Walled Struct. **94**, 45–55 (2015)
43. Xu, F.; Zhang, S.; Wu, K.: Dynamic crashing behavior of thin-walled conical tubular structures with nonlinearly-graded diameters. Proc. Inst. Mech. Eng. C J. Mech. Eng. Sci. **233**(7), 2456–2466 (2019)
44. Ragland, C.L.; Fessahaie, O.; Elliott, D.: Evaluation of frontal offset/oblique crash test conditions. In: Proceedings of 17th International Technical Conference on the Enhanced Safety of Vehicles CD ROM, Amsterdam, Netherlands (2001)
45. Bigdeli, A.; Nouri, M.D.: A crushing analysis and multi-objective optimization of thin-walled five-cell structures. Thin-Walled Struct. **137**, 1–18 (2019)
46. Li, Z.; Chen, R.; Lu, F.: Comparative analysis of crashworthiness of empty and foam-filled thin-walled tubes. Thin-Walled Struct. **124**, 343–349 (2018)
47. Pirmohammad, S.; Marzdashti, S.E.: Crushing behavior of new designed multi-cell members subjected to axial and oblique quasi-static loads. Thin-Walled Struct. **108**, 291–304 (2016)
48. Zarei, H.R.; Kröger, M.: Bending behavior of empty and foam-filled beams: structural optimization. Int. J. Impact Eng. **35**(6), 521–529 (2008)
49. Yin, H.; Chen, C.; Hu, T.; Wen, G.: Optimisation for bending crashworthiness of functionally graded foam-filled cellular structure. Int. J. Crashwortnhiess **23**(4), 446–460 (2017)
50. Yin, H.; Xiao, Y.; Wen, G.; Qing, Q.; Wu, X.: Crushing analysis and multi-objective optimization design for bionic thin-walled structure. Mater. Des. **87**, 825–834 (2015)
51. Hou, S.; Li, Q.; Long, S.; Yang, X.; Li, W.: Crashworthiness design for foam filled thin-wall structures. Mater. Des. **30**(6), 2024–2032 (2009)
52. Wierzbicki, T.; Abramowicz, W.: On the crushing mechanics of thin walled structures. J. Appl. Mech. **50**, 727–734 (1983)
53. Abramowiczt, W.; Jones, N.: Dynamic axial crushing of square tubes. Int. J. Impact Eng. **2**(2), 179–208 (1984)
54. Hanssen, A.G.; Langseth, M.; Hopperstad, O.S.: Static and dynamic crushing of square aluminium extrusions with aluminium foam filler. Int. J. Impact Eng. **24**, 347–283 (2000)
55. Liu, S.; Tong, Z.; Tang, Z.; Liu, Y.; Zhang, Z.: Bionic design modification of non-convex multi-corner thin-walled columns for improving energy absorption through adding bulkheads. Thin-Walled Struct. **88**, 70–81 (2015)
56. Huang, Z.; Zhang, X.: Three-point bending collapse of thin-walled rectangular beams. Thin-Walled Struct. **144**, 461–479 (2018)
57. Santosa, S.; Banhart, J.; Wierzbicki, T.: Experimental and numerical analyses of bending of foam-filled sections. Acta Mech. **148**(1), 199–213 (2001)
58. Lai, Y.; Jiang, X.; Fang, L.; Li, M.; Li, G.: Detailed explanation of isight parameter optimization theory and examples. Beijing University of Aeronautics and Astronautics Press, Beijing (2012)
59. Rayegani, A.; Nouri, G.: Seismic collapse probability and life cycle cost assessment of isolated structures subjected to pounding with smart hybrid isolation system using a modified fuzzy based controller. Structures **44**, 30–41 (2022)
60. Ehrgott, M.: Multiobjective optimization. AI Mag. **29**(4), 47–57 (2008)
61. Fang, J.; Gao, Y.; Sun, G.; Zhang, Y.; Li, Q.: Parametric analysis and multiobjective optimization for functionally graded foam-filled thin-wall tube under lateral impact. Thin-Walled Struct. **90**, 265–275 (2014)